Achievement of ion temperatures in excess of 100 million degrees Kelvin in the compact high-field spherical tokamak ST40

S. A. M. McNamara,[1] O. Asunta, J. Bland, P. Buxton, C. Colgan, A. Dnestrovskij, M. Gemmell, M. Gryaznevich, D. Hoffman, H. Lowe, R. Mirfayzi, G. Naylor, V. Nemytov, J. Njau, T. Pyragius, A. Rengle, M. Romanelli, C. Romero, M. Sertoli, V. Shevchenko, J. Sinha, A. Sladkomedova, S. Sridhar, Y. Takase, P. Thomas, J. Varje, B. Vincent, H. Willett, J. Wood, D. Zakhar

D. Battaglia, S.M. Kaye, L. Delgado-Aparicio, R. Maingi, D. Mueller, M. Podesta[2]

E. Delabie, B. Lomanowski[3]

O. Marchuk[4]

[1] *Tokamak Energy Ltd, Milton Park, Oxfordshire OX14 4SD, UK*
[2] *Princeton Plasma Physics Laboratory, Princeton, New Jersey 08543, USA*
[3] *Oak Ridge National Laboratory, Oak Ridge, Tennessee 37831, USA*
[4] Institut fur Plasmaphysik, Forschungszentrum Jülich, 52425, Julich, German

(Received day month year; accepted day month year; published day month year)

Ion temperatures of over 100 million degrees Kelvin (8.6keV) have been measured in the ST40 compact high-field spherical tokamak. Such high ion temperatures have not previously been reached in any spherical tokamak and have only been obtained in much larger devices with substantially more plasma heating power. In ST40 these plasmas operated in hot-ion-mode with a plasma current of 0.6MA, on-axis toroidal field of 1.9T, major radius of 0.45m, aspect ratio of 1.65, plasma volume of 0.9m^3, 1.8MW of injected neutral beam power, line averaged electron density of 4x10^{19}m^{-3} and electron temperature of 3keV.

Introduction – Spherical tokamaks (STs) have several beneficial features which make them an attractive option for commercial fusion power production. STs have a plasma aspect ratio (the ratio of the major to minor radii of the plasma torus) of less than approximately two and exhibit enhanced stability properties[1], as well as displaying more favourable transport and confinement properties than those observed in large aspect ratio tokamaks[2]. Recent advances in the development of high-field magnets made from high temperature superconductor (HTS), combined with the fundamentally favourable properties of the spherical tokamak, opens a route to smaller size and potentially reduced cost fusion power plants. Tokamak Energy Ltd, a private company based in Oxfordshire, UK, is developing commercial fusion power plants based on this approach.

Part of this development includes advancing the physics basis for the high-field ST towards commercial fusion using the ST40 tokamak. ST40 is a compact high-field spherical tokamak with copper magnets. In this letter we describe results from ST40, demonstrating the achievement of central ion temperatures above 100 million degrees Kelvin (8.6keV), which was the primary milestone for the recent phase of ST40 operations. By injecting 1.8MW of deuterium neutral beams into a deuterium plasma of volume 0.9m^3, with plasma current I_P=0.6MA and on-axis toroidal magnetic field of B_T=1.9T, carbon ion temperatures of 9.2keV were measured using a charge exchange recombination spectroscopy (CXRS) system where the most central line of slight measures slightly off the magnetic axis. This corresponds to central impurity temperatures of 9.8keV inferred using diagnostic forward models and to main ion

[1] Peng, YK M., and Dennis J. Strickler. "Features of spherical torus plasmas." Nuclear Fusion 26.6 (1986): 769.

[2] Kaye, Stanley M., Jack W. Connor, and Colin M. Roach. "Thermal confinement and transport in spherical tokamaks: A review." Plasma Physics and Controlled Fusion (2021).

temperature of 9.6keV estimated using TRANSP[3]. The error of the CXRS measured value is below 5%, while the uncertainty inferred values for the central temperatures (impurity and hydrogenic) is below 10%. This is the highest ion temperature achieved so far in a spherical tokamak or any tokamak of comparable size. Equivalent ion temperatures have only previously been obtained on devices with plasma volumes greater than fifteen times larger than ST40 and with substantially more plasma heating power[4]. For these discharges the fusion triple product is calculated to be $n_{i0}T_{i0}\tau_E \approx 6 \pm 2 \times 10^{18}\mathrm{m}^{-3}\mathrm{keVs}$.

These temperatures were achieved in hot-ion-mode scenarios, where the ion temperature exceeds that of the electrons, typically by a factor of two or greater, $T_i \gg T_e$. Hot-ion modes have been explored in several tokamaks[5, 6, 7, 8] and generally share common features of peaked density profiles, centralised ion heating, suppression of turbulence leading to improved ion confinement, and low ion-electron collisional coupling to minimise power transfer from the hotter ions to cooler electrons.

ST40 description – Typical ST40 plasma parameters are, major radius R_{Geo}≈0.4-0.5m; aspect ratios between A≈1.6-1.9; plasma currents ranging from I_P≈0.4-0.8MA and on-axis toroidal magnetics fields of B_T≈1.5-2.2T. Plasma heating is provided by two neutral beams injected tangentially in the co-current direction that deliver approximately 1MW at 55kV and 0.8MW at 24kV when operated in deuterium. Plasma start-up is via merging compression (MC), where two high-voltage in-vessel poloidal field coils inductively initiate the plasma[9]. MC is a robust start-up scheme that allows direct access to high plasma currents without the use of the central solenoid. A modest central solenoid, providing approximately 200mVs of inductive flux, is used to further increase the plasma current and sustain the current flat-top, which can last up to 200ms.

ST40 is equipped with numerous diagnostics. A full set of magnetic field and flux sensors are used for real-time magnetic control and post-pulse magnetic reconstruction. The plasma position and shape are determined in real-time using an in-house reconstruction code, PFIT, which estimates the plasma current centroid position. Between shots, magnetics-only equilibrium reconstruction is produced with EFIT[10]. The electron density is measured using two interferometers, a sub-millimetre (SMM) and a near-infrared (NIR) system operating at 1mm and 1μm+1.5μm, and measuring along a radial and a tangential midplane line of sight respectively. A visible survey spectrometer and line-filtered diodes (D_α, D_β, C-II, C-III, O-II, O-III) are used for low-Z impurity and Bremsstrahlung monitoring, and a tangential viewing soft X-ray (SXR) camera with 10μm Be-window provides information on the radiated power. A 15-channel neutral particle analyser (NPA) measuring neutral hydrogenic particle fluxes at energies between 1-41keV provides information on the fast ion distribution function. High-resolution fast visible (10kHz) and D_α (1kHz) cameras view the main chamber and upper/lower divertors. An IR camera views the central column and parts of the divertor regions.

A high-resolution X-ray crystal spectrometer (XRCS) diagnostic, measures electron and ion temperatures in the core region and requires a small prefill puff of argon in every shot. A visible charge-exchange recombination spectroscopy (CXRS) system, viewing the C-VI 529nm n=8-7 spectral line, measures ion temperature and toroidal rotation profiles along 6 lines of sight intersecting the 24keV heating neutral beam.

High ion temperature scenario – **Error! Reference source not found.** shows waveforms of the main plasma parameters of an ST40 pulse designed to maximise the ion temperature. Merging-compression was used to initiate the plasma and established an approximately circular centre column

[3] J. Breslau, M. Gorelenkova, F. Poli, J. Sachdev, A. Pankin, and G. Perumpilly, TRANSP, US-DoE Computer Software, https://doi.org/10.11578/dc.20180627.4 (2018).

[4] Verdoolaege, Geert, et al. "The updated ITPA global H-mode confinement database: description and analysis." Nuclear Fusion 61.7 (2021): 076006.

[5] Eubank, H., et al. "Neutral-beam-heating results from the Princeton Large Torus." Physical Review Letters 43.4 (1979): 270.

[6] Söldner, F. X., et al. "Approach to steady state high performance in DD and DT plasmas with optimized shear in JET." Nuclear fusion 39.3 (1999): 407.

[7] Mansfield, D. K., et al. "Enhancement of Tokamak Fusion Test Reactor performance by lithium conditioning." Physics of Plasmas 3.5 (1996): 1892-1897.

[8] Kishimoto, H., et al. "Advanced tokamak research on JT-60." Nuclear fusion 45.8 (2005): 986.

[9] Gryaznevich, M. P., and A. Sykes. "Merging-compression formation of high temperature tokamak plasma." Nuclear Fusion 57.7 (2017): 072003.

[10] Lao, L. L., et al. "Reconstruction of current profile parameters and plasma shapes in tokamaks." Nuclear fusion 25.11 (1985): 1611.

limited plasma with I_P=0.45MA and R_{Geo}=0.40m at 10ms.

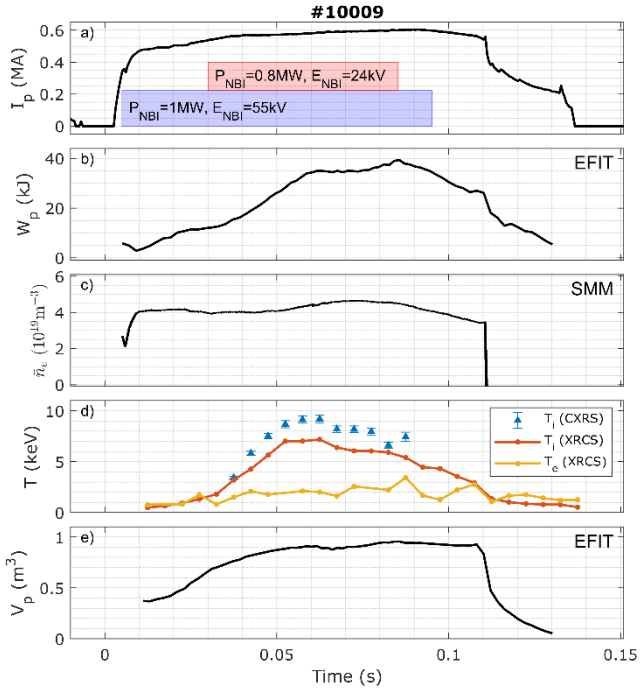

FIG. 1 Overview of discharge designed to maximise central ion temperature. Shown are (a) plasma current and neutral beam injection, (b) EFIT stored energy, (c) line averaged electron density, (d) ion and electron temperature measured by XRCS and CXRS diagnostics, and (e) plasma volume from EFIT magnetic reconstruction.

MC was followed by a fast current ramp phase where the plasma current was increased at a rate of 4MA/s to 0.57MA between 10-40ms (**Error! Reference source not found.** (*a*)) using the central solenoid, while the plasma size was allowed to increase to R_{Geo}=0.45m with an elongation κ=1.5, aspect ratio A=1.65, and plasma volume of V_p=0.9m^3. At the end of the fast ramp the plasma is in a double null diverted configuration with a slight bias towards the lower divertor. The equilibrium shape is influenced by induced currents in a set of passive stabilisers mounted behind each divertor plate and around the upper and lower section of the centre column. A magnetic reconstruction at the time of maximum ion temperature is shown in FIG. 2. By this time the induced currents in the passive stabilisers have reduced and the plasma becomes marginally limited on the centre column, but with minimal interaction.

Injection of the 55kV neutral beam began 5ms before the start of the fast current ramp phase (**Error! Reference source not found.** (*a*)), which allowed the beam current to reach the maximum level by 10ms, and together with the ohmic heating maintained a core electron temperature of around 1.5keV, as measured using the XRCS diagnostic (**Error! Reference source not found.** (*d*)). The 55kV beam fuelling maintained an approximately constant line averaged electron density of 4x10^{19}m^{-3} (**Error! Reference source not found.** (*c*)) without the need for gas puff fuelling, which would have resulted in a broadening of the density profile and neutral beam deposition profile. Because of this, gas puff fuelling was only used during plasma start-up. During the rest of the pulse. For obtaining highest ion temperatures, the optimum line averaged electron density at the start of the 24kV beam injection was found to be around 4x10^{19}m^{-3}. At this density, the ion-electron collisional coupling is sufficiently low and the fraction of absorbed beam power sufficiently high to enable access to hot-ion-modes, with measured ion to electron temperature ratios of T_i/T_e≈3-4. The density after merging compression could be set by adjusting the pre-breakdown fuelling and duration of the intershot helium glow discharge cleaning (HeGDC). 5 minutes of intershot HeGDC was found to be sufficient to reduce the wall fuelling source from the graphite plasma facing components to a level where the target density could be achieved. Routine boronisations were also performed, which reduced impurity influx and substantially reduced the oxygen content and the Bremsstrahlung emission.

This high heating power phase started at 30ms with the injection of the 24kV beam (**Error! Reference source not found.** (*a*)), which remained on until 85ms. During this phase, the plasma current was gradually increased to 0.6MA at a rate of approximately 0.6MA/s. The combination of increased T_e, modest n_e, an increase in plasma cross-section and the fast plasma current ramp after merging compression all served to delay the onset of sawteeth, which otherwise limited the central ion temperature. Higher plasma currents of I_P=0.8MA were achieved during the programme. However, the optimum I_P for accessing high ion temperatures was found to be around 0.6MA. Higher plasma currents advanced the onset of sawteeth and increased particle confinement resulting in higher densities, which led to a reduction in the peak ion temperature due to increased collisional coupling between ions and electrons. During both the plasma current ramp-up and high heating power phases the plasma remained in L-mode.

The injection of the 24kV beam caused the ion temperature to increase rapidly (**Error! Reference source not found.** (*d*)). The argon impurity

temperature measured by the XRCS increased from 1.5keV to 7keV in 25ms. At its peak at 58ms, the CXRS diagnostic measured a carbon ion temperature of 9.2keV by which point the stored energy had increased to 35kJ. Due to its lower injection energy, this beam also provided more fuelling, resulting in an increase in the line averaged electron density to $4.5 \times 10^{19} m^{-3}$ (**Error! Reference source not found.** (*c*)). This additional fuelling was during a period where the plasma volume was increasing, which offset the increase in the line averaged density. This increase in density reduced the measured ion temperature by around 1keV and led to a ~0.5keV increase in electron temperature, due to the increased ion-electron coupling. The stored energy continued to rise, peaking at 40kJ at the end of the high-power phase.

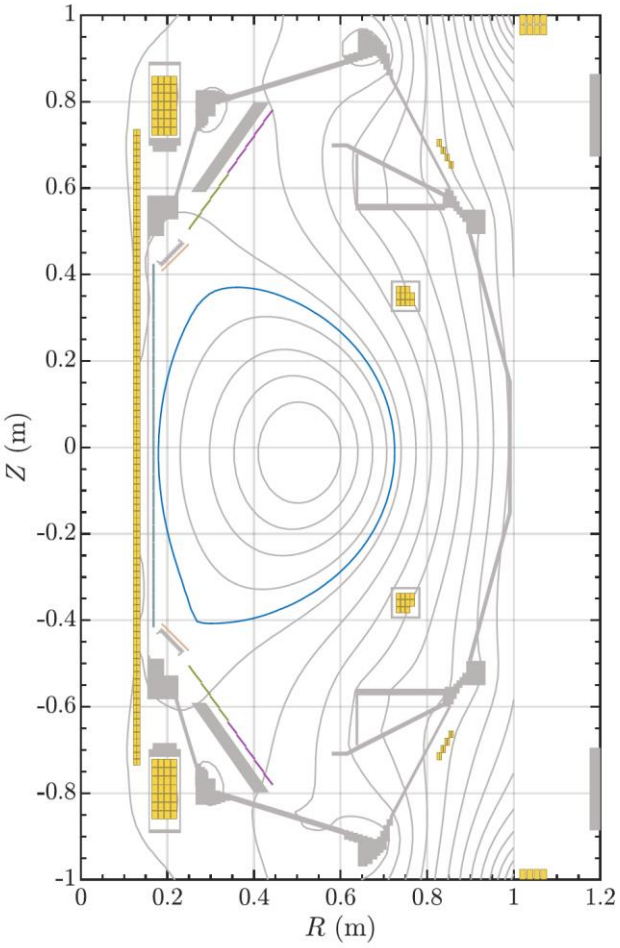

FIG. 2 Plasma magnetic equilibrium reconstruction computed using EFIT at the time of maximum ion temperature for pulse #10009.

Interpretation of results – Given the currently limited availability of profile diagnostics, the main plasma profile shapes have been constrained using an integrated analysis workflow. This workflow employs forward models of the XRCS, CXRS and interferometer diagnostics, makes use of ASTRA-NUBEAM[11] to determine fast particle contributions, uses EFIT equilibrium reconstruction for remapping and to constrain the equilibrium stored energy, and computes the main ion temperatures from the impurity temperatures using TRANSP.

For the XRCS diagnostic, He-like Ar spectra have been modelled using atomic data[12], which includes all the relevant He and Li-like transitions. The CXRS diagnostic model uses FIDASIM[13] for the beam characterization and atomic data from OPEN-ADAS[14] for the spectra, including cross-section effects in the calculation.

Starting from initial assumptions about the trialled profile shapes and boundary conditions at the separatrix, the workflow determines the possible plasma profile combinations by comparing modelled and experimental quantities. The electron density profile is re-scaled to match the line of sight integral of the SMM and NIR interferometers, and the electron temperature is optimized to match the experimental values of the argon line ratios measured from XRCS. The ion temperature, assuming identical temperatures for C and Ar, is optimised for both the CXRS measurements of the active C-VI spectra and the XRCS measurement of the He-like Ar spectra. Toroidal rotation is optimized to match the values measured by CXRS. These profiles are then fed into an interpretive ASTRA-NUBEAM simulation which calculates, amongst other things, the power balance, the fast particle pressure, total stored energy and loop voltage. The stored energy is compared with the value from EFIT and, if the modelled stored energy is within 20% of the measured value, the profile combination is retained as a possible solution, otherwise it is discarded.

Multiple independent runs of this workflow are performed, testing broad and peaked profile shapes and their combinations. This leads to a selected set of potential profile shapes which are combined to give a confidence band (FIG. 3).

For all analysis runs, C and He concentrations are assumed to be constant across the radius and in time

[11] Pankin, Alexei, et al. "The tokamak Monte Carlo fast ion module NUBEAM in the National Transport Code Collaboration library." Computer Physics Communications 159.3 (2004): 157-184.
[12] Plasma Phys. Control. Fusion 48 (2006) 1633–1646
[13] Geiger, B., et al. "Progress in modelling fast-ion D-alpha spectra and neutral particle analyzer fluxes using FIDASIM." Plasma Physics and Controlled Fusion 62.10 (2020): 105008.
[14] https://open.adas.ac.uk/

(at 3% and 1% respectively). The Ar concentration is set to follow the time evolution of the He-like w-resonance line, using a rough cross-calibration vs. Bremsstrahlung emission performed during dedicated pulses with and without Ar puffs. Values typically don't exceed 0.1%. The trialled Ar density profile shapes include a flat concentration assumption and a very peaked profile. The latter leads to more conservative estimate of the central temperatures from the XRCS weighing the emission shell further towards the plasma centre. Effects of impurity transport have been investigated but found to be of second order in comparison to the uncertainties in the profile shapes, which are accounted for in the model.

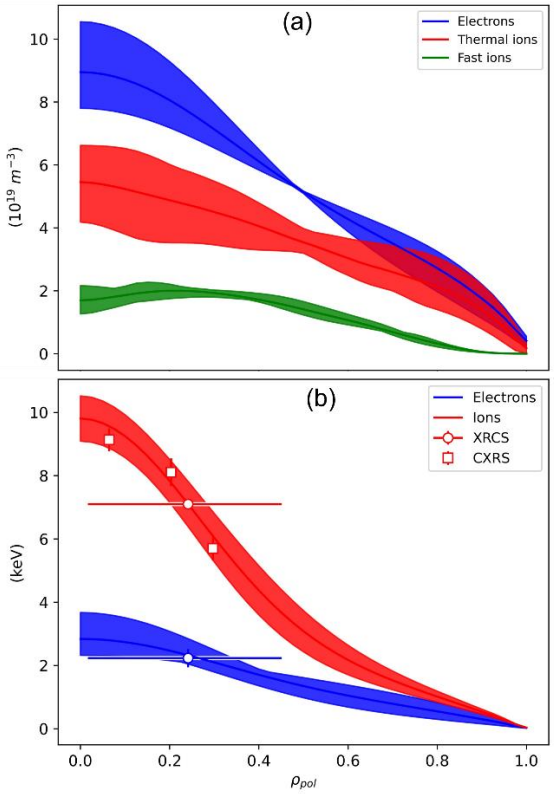

FIG. 3 Profiles of (a) electron density, ion and fast particle densities, (b) ion and electron temperature determined using the integrated analysis approach for pulse #10009 at time of maximum ion temperature (58ms). Squares and circles in (b) are the measured temperatures from CXRS and XRCS, respectively, the horizontal line is the integration region of the XRCS measurement calculated as the 2nd moment of the He-like Ar resonance line emission shell.

Sensitivity studies and detailed experiments have shown that neither the XRCS or the CXRS are affected by rotation shearing or temperature smearing and that the experimental measurements represent lower limits of the central values for XRCS and of the local values at the intersection between the beam and the line of sights for the CXRS.

The final temperature and density profiles for pulse #10009 at the time of peak ion temperature, 58ms, are shown in **Error! Reference source not found.**. The range of profiles shown are the retained sets from the integrated analysis that lead to a satisfactory match with the experimental data. The resulting fast particle density, as calculated from ASTRA-NUBEAM (green profile in FIG. 3 (*a*)), is around a factor of three lower than the thermal main ion density (red profile in FIG. 3 (*a*)). Finally, TRANSP is used to calculate the thermal hydrogenic temperatures, which can differ from that of the measured impurities in plasmas with significant fast-particle fractions and low toroidal rotation. The inferred central toroidal rotations from CXRS are around 220 km/s, but the profile shape and the central values are less precise than the ion temperature due to systematic uncertainties in lines of sight and beam geometry. To address this, independent TRANSP runs have been performed with high and low central toroidal rotations of 260 km/s and 160 km/s, using the ion temperature profile shape as reference. The resulting central deuterium temperature is, in both cases, only slightly lower than that of the impurities, with a value of 9.6$\pm$0.4 keV for the high rotation case, which decreases of about 0.2 keV if low rotation is assumed.

Taking the range of profiles above, the values of the absorbed neutral beam, P_{NB}, and Ohmic, P_{OH}, heating powers and thermal stored energy computed by ASTRA, W_{th}, and defining the energy confinement time as $\tau_E = W_{th}/(P_{NB} + P_{OH} - dW_{th}/dt)$, the fusion triple product is calculated to be $n_{i0}T_{i0}\tau_E \approx 6 \pm 2 \times 10^{18}\mathrm{m}^{-3}\mathrm{keVs}$.

Conclusions – We have reported on the attainment of central ion temperatures of 9.6keV and corresponding fusion triple product of $n_{i0}T_{i0}\tau_E \approx 6 \pm 2 \times 10^{18}\mathrm{m}^{-3}\mathrm{keVs}$ in the ST40 tokamak and demonstrated for the first time that fusion relevant ion temperatures can be achieved in a compact, high field, spherical tokamak.

Acknowledgements – We gratefully acknowledge the hard work and dedication of the ST40 team; the support of the Tokamak Energy Board and shareholders; the guidance and scrutiny of the independent Diagnostics Advisory Board chaired by Alan Costley and attended by Kieron Gibson, Patrick Carolan, Jo Lister, Manfred von Hellermann, Francesco Orsitto and Tom Todd; and the contributions from collaborators at Princeton Plasma

Physics Laboratory and Oak Ridge National Laboratory that were supported through U.S. Department of Energy CRADA NFE-19-07769.